

## Supporting Information

### Self-assembled polycarbazole microspheres as single-component, white-colour resonant photoemitters

Soh Kushida, Shinnosuke Okabe, Thang D. Dao, Satoshi Ishii, Tadaaki Nagao, Akinori Saeki, Masashi Kijima and Yohei Yamamoto\*

\* To whom correspondence should be addressed.  
E-mail: yamamoto@ims.tsukuba.ac.jp

#### Table of Contents

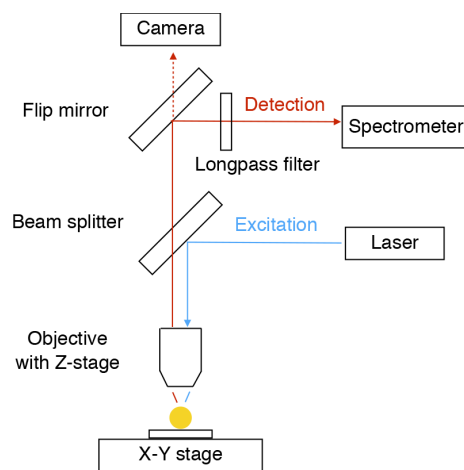
<b>1. Materials and measurements</b> -----	<b>S2</b>
<b>2. <math>\mu</math>-PL measurements</b> -----	<b>S3</b>
<b>3. Simulations of WGM PL</b> -----	<b>S4</b>
<b>4. Supporting Figures and Tables</b> -----	<b>S5</b>
<b>5. Supporting References</b> -----	<b>S9</b>

## 1. Materials and measurements

Unless otherwise noted, reagents and solvents were used as received from Aldrich Chemical Co. Ltd, Tokyo Chemical Industry Co. Ltd and Nakarai Tesque Co. Polycarbazoles **P1–P5** were synthesized according to the reported procedures.<sup>S1</sup> The representative good solvents for these polymers are CHCl<sub>3</sub>, CH<sub>2</sub>Cl<sub>2</sub>, and THF, and the poor solvents are MeOH and MeCN. NMR spectra were recorded on a JEOL ECS-400 (400 MHz) spectrometer by using tetramethylsilane (0 ppm for <sup>1</sup>H NMR) as an internal standard. Gel permeation chromatography (GPC) was performed in CHCl<sub>3</sub> solution using a Shimadzu LC-solution GPC system equipped with a Phenogel 5u 10E4A and a guard columns (Phenomenex) and a SPD-20A UV-vis detector and a LC-6AD pump. Molecular weight (*M<sub>n</sub>*) and polydispersity index (PDI) of the polymer samples were calculated on the basis of a polystyrene calibration. Photoabsorption and steady-state PL spectra were recorded on a JASCO V-630 spectrophotometer and a JASCO FP-8500 spectrofluorometer, respectively. Thin films of polymers were prepared by drop casting from CHCl<sub>3</sub> solution. SEM microscopy was performed on a Hitachi model SU-8000 FE-SEM and JEOL model JSM-5610 SEM operating at 10 and 20 kV, respectively. Silicon was used as a substrate and Au for coating. Ellipsometry measurements were carried out on a J. A. Woollam Japan model M-2000 spectroscopic ellipsometer using 3–5 μm-thick polymer films. Picosecond time-resolved fluorescence lifetime measurements were performed by using time-correlated single photon counting (TCSPC) lifetime spectroscopy system of a HORIBA model FluoroCube 3000U-UltraFast-SP spectrophotometer equipped with an excitation laser NanoLED-375L (< 200 ps, repetition rate of 1 MHz, λ<sub>ex</sub> = 377 nm). ESR spectra were recorded at 25 °C on a Bruker model EMX-T ESR Spectrometer. Attenuated total reflection (ATR) Fourier transform infrared (FT-IR) spectra were recorded at 25 °C with a JASCO model FT/IR-4200 Fourier transform infrared spectrometer equipped with a model PR0450-S ATR attachment. For sample preparation, a CHCl<sub>3</sub> solution of **P1** was drop-cast onto the ATR stage and air-dried. The sample film was directly irradiated by CNI model MPL-F-355 pulsed laser (λ<sub>ex</sub> = 355 nm, 10 mW, 1 kHz) with the irradiation time of 1 h.

## 2. $\mu$ -PL measurements

$\mu$ -PL measurements were carried out using a  $\mu$ -PL measurement system (schematic illustration of the experimental setup is drawn below).<sup>S2</sup> An optical microscope was used with a long-distance 100x objective (NA = 0.8) to identify suitable particles and determine their diameters ( $d$ ). For measurements, a WITec  $\mu$ -PL system was used with a model Alpha 300S microscope combined with a Princeton Instruments model Action SP2300 monochromator (grating: 300 grooves  $\text{mm}^{-1}$ ) and an Andor iDus model DU-401A BR-DD-352 CCD camera cooled to  $-60$  °C. The perimeter of a single sphere was photoexcited at 25 °C under ambient conditions by an HU ANIC model DH405-10-5 CW laser with the wavelength, power, integration time, and spot size of 405 nm, 10 mW, 0.1 s, and  $\sim 0.5$   $\mu\text{m}$ , respectively.



### 3. Simulations of WGM PL

The simulations of the WGM emission are conducted using Equations S1 and S2 for transverse electric (TE) and magnetic (TM) mode emissions, respectively<sup>S3</sup>;

$$\lambda_n^E = 2\pi r (\varepsilon\mu)^{\frac{1}{2}} \left[ \left(n + \frac{1}{2}\right) + 1.85576 \left(n + \frac{1}{2}\right)^{\frac{1}{3}} - \frac{1}{\varepsilon} \left(\frac{\varepsilon\mu}{\varepsilon\mu - 1}\right)^{\frac{1}{2}} \right]^{-1} \quad (\text{S1})$$

$$\lambda_n^H = 2\pi r (\varepsilon\mu)^{\frac{1}{2}} \left[ \left(n + \frac{1}{2}\right) + 1.85576 \left(n + \frac{1}{2}\right)^{\frac{1}{3}} - \frac{1}{\mu} \left(\frac{\varepsilon\mu}{\varepsilon\mu - 1}\right)^{\frac{1}{2}} \right]^{-1} \quad (\text{S2})$$

where  $\lambda_n^E$  and  $\lambda_n^H$  are the wavelengths of the  $n$ -th TM and TE mode photoemission, respectively,  $\varepsilon$  ( $= \eta^2$ ) is the dielectric permittivity,  $\mu$  ( $= 1$ ) is the magnetic permeability, and  $r$  is the sphere's radius. Here, the much higher order term was neglected. The average  $\eta$  values for **P1** ( $\sim 1.55$ ) and **P2** ( $\sim 1.58$ ) were obtained by spectroscopic ellipsometry measurements (Fig. S3). For the simulation of the emission lines, TM and TE modes were calculated using the equations S1 and S2. Within the margin of error of the sphere's radius (given by optical microscopy), the simulation adapts the radius so that both TM and TE modes agree well for given orders  $n$ , effectively determining the radius with much higher precision.

## 4. Supporting Figures and Tables

**Table S1.** Number-average molecular weight ( $M_n$ ), polydispersity index (PDI), degree of polymerization (D. P.), maximum wavelength of photoabsorption ( $\lambda_{\text{abs}}$ ) and PL ( $\lambda_{\text{em}}$ ) in  $\text{CHCl}_3$  and for cast films, band gap energy ( $E_g$ ), PL quantum yield ( $\phi_{\text{PL}}$ ) in  $\text{CHCl}_3$  and for cast films, and decomposition temperature ( $T_d$ ; 5%-weight loss temperature) of **P1** and **P2**.

	$M_n / 10^3$ $\text{g mol}^{-1}$	PDI	D. P.	$\lambda_{\text{abs}} / \text{nm}$		$\lambda_{\text{em}} / \text{nm}$		$E_g /$ $\text{eV}$	$\phi_{\text{PL}}$		$T_d / ^\circ\text{C}$
				in $\text{CHCl}_3$	film	in $\text{CHCl}_3$	film		in $\text{CHCl}_3$	film	
<b>P1</b>	67	3.92	123	391	390	420	427	2.96	0.80	0.21	389
<b>P2</b>	29	3.41	55	383	384	418	430	2.90	0.78	0.16	391

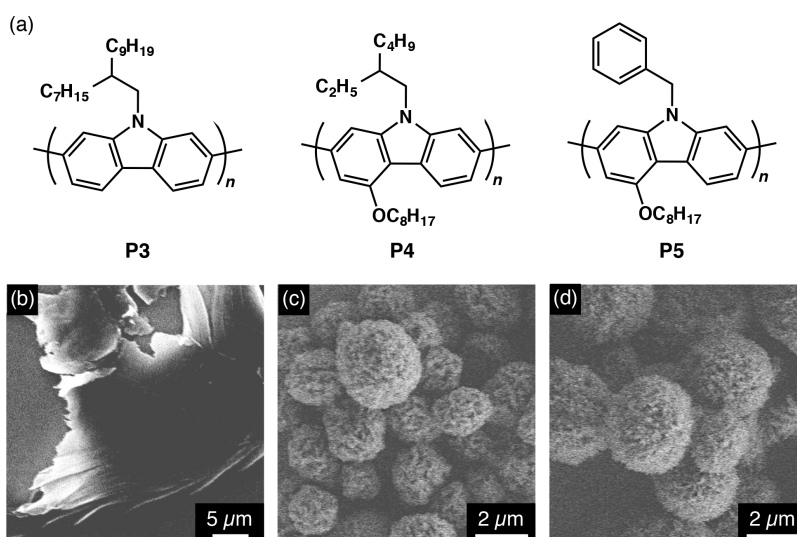


**Fig. S1.** (a) Molecular structures of poly(2,7-carbazole) **P3**–**P5**. (b–d) SEM micrographs of self-assembled precipitates of **P3** (b), **P4** (c), and **P5** (d).

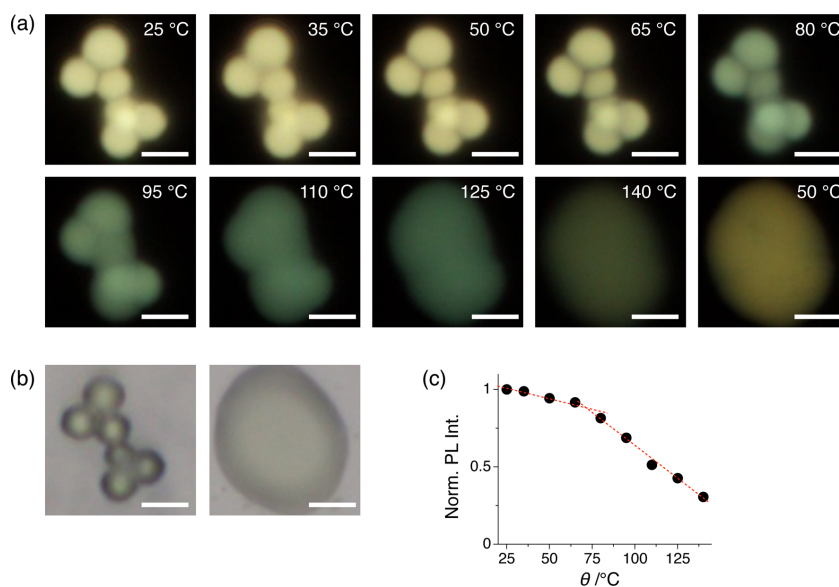


**Fig. S2.** (a) Fluorescent microscope images of the microspheres of **P1** upon heating from 25 °C to 140 °C and then cooling to 50 °C. Scale bar: 20  $\mu\text{m}$ . (b) Optical microscope images of the microspheres of **P1** before and after annealing to 140 °C. Scale bar: 20  $\mu\text{m}$ . (c) Plot of the normalized PL intensity versus temperature upon heating.

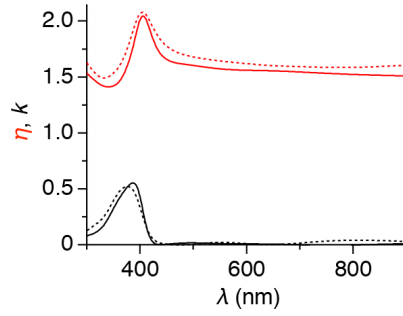


**Fig. S3.** Spectroscopic ellipsometry profiles of cast films of **P1** (solid lines) and **P2** (broken lines). Red and black lines indicate  $\eta$  and  $k$ , respectively.

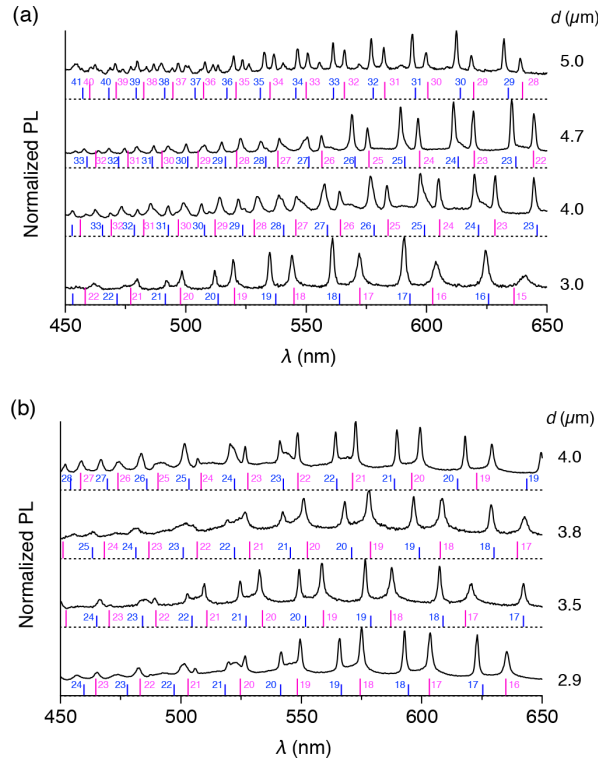


**Fig. S4.** PL spectra of a single microsphere of **P1** (a) and **P2** (b) with different  $d$ . The pink and blue lines below the spectra shows wavelengths simulated by using Equations S1 and S2 for TE and TM modes, respectively, and the numbers are the corresponding WGM indices.

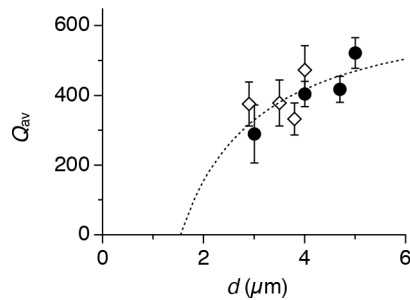


**Fig. S5.** Plots of Q-factors versus  $d$  for microspheres of **P1** (black) and **P2** (squares). Error bars show standard deviations. The broken curves indicate the exploration of the least squares fit to the phenomenological equation;  $Q = -1049 d^{-1} + 680$ .

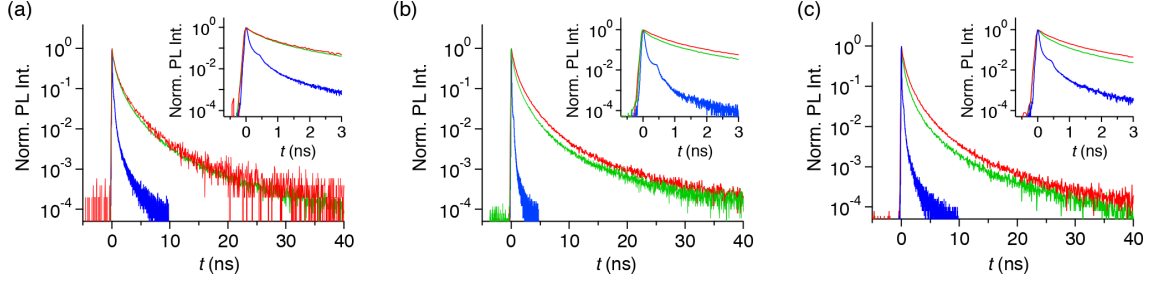


**Fig. S6.** PL decay profiles of a thin film of microspheres of **P2** (a) and cast films from  $\text{CHCl}_3$  solution of **P1** (b) and **P2** (c).  $\lambda_{\text{ex}} = 377$  nm. Blue, red, and green profiles indicate PL decay at 450, 550, and 650 nm, respectively.

**Table S2.** PL lifetimes at 450, 550, and 650 nm, simulated by bi- or tri-exponential fittings of the decay profiles.  $\tau_n$  and  $f_n$  ( $n = 1-3$ ) are the lifetime and fraction of each component, respectively. The average PL lifetime ( $\tau_{\text{av}}$ ) is calculated using the  $\tau_n$  and  $f_n$  values.

**P1 (Microspheres)**

$\lambda_{\text{em}} / \text{nm}$	$\tau_1 / \text{ns} (f_1)$	$\tau_2 / \text{ns} (f_2)$	$\tau_3 / \text{ns} (f_3)$	$\tau_{\text{av}} / \text{ns}^a$
450	0.026 (0.650)	0.220 (0.262)	1.317 (0.088)	0.191
550	0.265 (0.262)	1.569 (0.738)	—	1.228
650	0.411 (0.371)	2.108 (0.557)	11.193 (0.073)	2.088

**P1 (Cast film from solution)**

$\lambda_{\text{em}} / \text{nm}$	$\tau_1 / \text{ns} (f_1)$	$\tau_2 / \text{ns} (f_2)$	$\tau_3 / \text{ns} (f_3)$	$\tau_{\text{av}} / \text{ns}^a$
450	0.025 (0.860)	0.108 (0.122)	0.790 (0.019)	0.048
550	0.209 (0.323)	1.265 (0.551)	6.413 (0.126)	1.572
650	0.394 (0.394)	1.838 (0.522)	9.442 (0.083)	1.902

**P2 (Microspheres)**

$\lambda_{\text{em}} / \text{nm}$	$\tau_1 / \text{ns} (f_1)$	$\tau_2 / \text{ns} (f_2)$	$\tau_3 / \text{ns} (f_3)$	$\tau_{\text{av}} / \text{ns}^a$
450	0.014 (0.759)	0.250 (0.187)	1.496 (0.055)	0.139
550	0.218 (0.328)	1.279 (0.534)	5.838 (0.138)	1.558
650	0.126 (0.203)	0.870 (0.503)	3.615 (0.294)	1.524

**P2 (Cast film from solution)**

$\lambda_{\text{em}} / \text{nm}$	$\tau_1 / \text{ns} (f_1)$	$\tau_2 / \text{ns} (f_2)$	$\tau_3 / \text{ns} (f_3)$	$\tau_{\text{av}} / \text{ns}^a$
450	0.017 (0.752)	0.136 (0.191)	0.905 (0.056)	0.090
550	0.173 (0.387)	1.027 (0.488)	5.241 (0.124)	1.220
650	0.284 (0.369)	1.456 (0.522)	6.729 (0.110)	1.602

<sup>a</sup>  $\tau_{\text{av}}$  is defined as  $(\tau_1 f_1 + \tau_2 f_2 + \tau_3 f_3) / (f_1 + f_2 + f_3)$

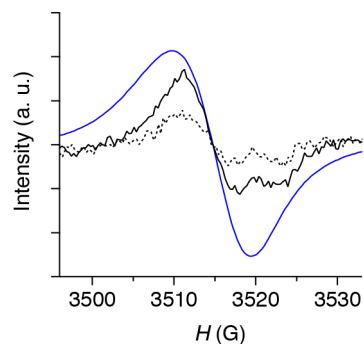


**Fig. S7.** ESR spectra of **P1** in dark (black, dotted), upon laser irradiation at 355 nm in  $N_2$  atmosphere (black, solid), and upon exposure to iodine vapour (blue).

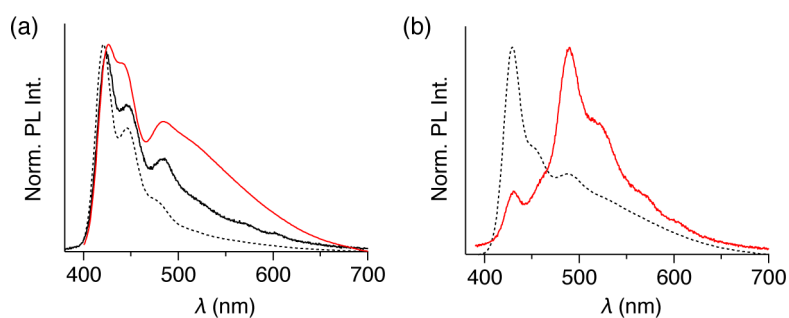


**Fig. S8.** PL spectra of **P1** (a) and **P3** (b) upon photoexcitation with stationary light before laser irradiation (black, dotted), after laser irradiation under  $N_2$  atmosphere (black, solid), and after laser irradiation in air (red).

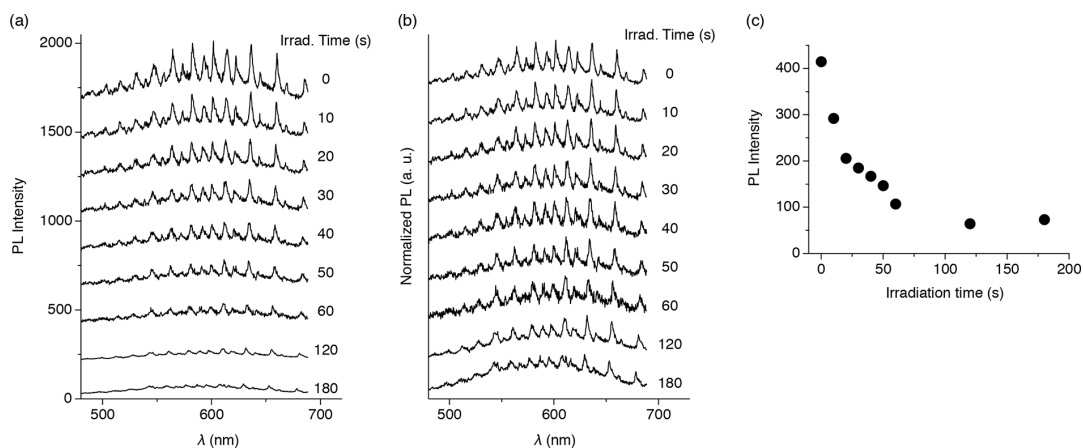


**Fig. S9.**  $\mu$ -PL spectral change upon laser irradiation to a single microsphere of **1**. (a) PL intensity versus  $\lambda$ . (b) Normalized PL intensity versus  $\lambda$ . (c) Plot of the PL peak intensity at  $\sim 600$  nm versus irradiation time.

## 5. Supporting References

- S1. T. Horii, T. Shinnai, K. Tsuchiya, T. Mori and M. Kijima, *J. Polym. Sci. A, Polym. Chem.*, 2012, **50**, 4557; K. Shibasaki, T. Yasuda, Y. Yamamoto and M. Kijima, *Polym. Chem.*, 2015, **6**, 5921; S. Okabe, K. Shibasaki and M. Kijima, *Polym. Preprints, Jpn*, 2015, **64**, 3Pa083.
- S2. S. Kushida, D. Braam, C. Pan, T. D. Dao, K. Tabata, K. Sugiyasu, M. Takeuchi, S. Ishii, T. Nagao, A. Lorke and Y. Yamamoto, *Macromolecules*, 2015, **48**, 3928.
- S3. A. N. Oraevsky, *Quant. Electron.* 2002, **32**, 377.